A Combination of Screening and Computational Approaches for the Identification of Novel Compounds That Decrease Mast Cell Degranulation

Marisa P. McShane[1], Tim Friedrichson[2], Angelika Giner[1], Felix Meyenhofer[1,3], Rico Barsacchi[1], Marc Bickle[1], and Marino Zerial[1]

Abstract

High-content screening of compound libraries poses various challenges in the early steps in drug discovery such as gaining insights into the mode of action of the selected compounds. Here, we addressed these challenges by integrating two biological screens through bioinformatics and computational analysis. We screened a small-molecule library enriched in amphiphilic compounds in a degranulation assay in rat basophilic leukemia 2H3 (RBL-2H3) cells. The same library was rescreened in a high-content image-based endocytosis assay in HeLa cells. This assay was previously applied to a genome-wide RNAi screen that produced quantitative multiparametric phenotypic profiles for genes that directly or indirectly affect endocytosis. By correlating the endocytic profiles of the compounds with the genome-wide siRNA profiles, we identified candidate pathways that may be inhibited by the compounds. Among these, we focused on the Akt pathway and validated its inhibition in HeLa and RBL-2H3 cells. We further showed that the compounds inhibited the translocation of the Akt-PH domain to the plasma membrane. The approach performed here can be used to integrate chemical and functional genomics screens for investigating the mechanism of action of compounds.

Introduction

The delivery of new drugs to the market has been declining in past years because of failures in clinical phase II and III trials that have caused a concomitant increase in the costs of drug development.[1] Part of the problem in drug discovery lies in the difficulty of analyzing how cellular networks are regulated, integrated, and respond to chemical perturbations. Initial efforts focused on gene expression profiling on drug treatment to create connectivity maps,[2] but more recently, phenotypic and high-content assays have been employed. Data have shown that phenotypic screening resulted in the development of more new drugs than with target-based assays.[3,4] However, many of these phenotypic screening assays do not use all of the information collected and are limited to only one or two parameters.[5] This is because the high level of complexity and large amount of data pose challenges for their analysis and interpretation. Nevertheless, the high complexity and granularity provide a means to identify the molecular pathways affected, just as in genetic screens the phenotypic alterations in a mutant are the signature of specific signaling pathways. With this complexity also arises the problem of defining hits and reducing the number of hits to a manageable number for follow-up studies. In phenotypic screening, two major obstacles, mechanism of action identification and hit definition, require novel methodologies to be developed, including computational approaches.

To improve hit and pathway identification, we used an approach based on the integration of chemical and functional genomics high-content screens. We have previously

[1]Max Planck Institute of Molecular Cell Biology and Genetics, Dresden, Germany
[2]JADO Technologies GmbH, Dresden, Germany
[3]University of Fribourg, Department of Medicine–Anatomy, Fribourg, Switzerland

Corresponding Author:
Marino Zerial, Max Planck Institute of Molecular Cell Biology and Genetics, Pfotenhauerstrasse 108, 01307 Dresden, Germany.
Email: zerial@mpi-cbg.de

conducted a genome-wide, image-based RNAi screen on the endocytosis and the endosomal distribution of two types of fluorescent cargo, epidermal growth factor (EGF) as a prototype for signaling cargo and transferrin (Tf), a recycling cargo, in HeLa cells.[6] An important feature of this screen was that the genes were profiled using a set of 62 quantitative parameters describing endocytic features such as the amount of total endocytosed cargo, the number of endosomes, size, the amount of cargo per endosome, and the intracellular position of the endosomes. This approach led to the identification of ~4600 genes involved in various pathways, including signaling and metabolism.[6] In principle, the multiparametric profiles obtained in the functional genomic screen could serve as reference profiles for a comparison with phenotypes induced by pharmacological perturbations. Indeed, such a comparison has been successfully applied to identify and characterize compounds that restore mycobacterium killing by the host.[7] By bridging functional genomics with compound screens, this method cannot identify the precise target protein(s) but can be used to predict pathways modulated by the compounds. How applicable this method is to other assays and cell types remains to be determined.

In this study, we wanted to further test whether the combination of chemical and genomic screens and computational approaches could be used to identify both hits and pathways modulated by the selected compounds. First, we addressed a biological process governed by signaling molecules partitioning in membrane microdomains and undergoing intracellular trafficking. We chose mast cell degranulation to modulate pharmacologically, which is highly relevant for both basic and applied research. During allergic reactions, mast cells degranulate and release histamine, the main causative agent for allergic symptoms.[8] Most therapeutics target the histamine-1 receptor using antihistamines, but other signaling receptors and pathways are involved in the allergic response. One particular pathway involves the binding of IgE to the receptor FCεRI, to release mediators, such as histamines and cytokines.[9] FCεRI has been shown to be endocytosed upon activation and reside in membrane microdomains.[10] We aimed to identify novel inhibitors of IgE-mediated degranulation of mast cells with an improved pharmacological profile compared with miltefosine, our internal reference compound. Miltefosine is a potent mast cell inhibitor in vitro and ex vivo and effective in the clinic in mast cell related diseases,[11,12] although it can induce adverse effects when administered systemically. Furthermore, to identify the pathways modulated by hit compounds, we screened the same library in an endocytosis assay and correlated the screen results using computational and bioinformatics analysis. The pathways identified were then tested in several cell lines to validate the predictions of our method.

Methods and Materials

Degranulation, Cytotoxicity Assays

The degranulation assay was as previously described.[13] Briefly, RBL-2H3 cells were lysed in 0.1 mL complete MSD lysis buffer/well (MSD Tris Lysis buffer containing phosphatase inhibitor 1, phosphatase inhibitor 2, protease inhibitor solution, and 2 mM PMSF) for 30 min at 4 °C with gentle agitation. Lysates were pooled and centrifuged 10 min with $10{,}000 \times g$ at 4 °C. Aliquots were taken for hexosaminidase measurement and determination of protein concentration. Lysates were aliquoted, snap-frozen in liquid nitrogen, and stored at –80 °C. The controls used are defined as follows: negative control was the supernatant of unstimulated cells measured for unspecific β-hexosaminidase release, positive control was the supernatant of DNP (dinitrophenyl)–human serum albumin (HSA)–stimulated cells measured for specific, antigen-stimulated β-hexosaminidase release, and the maximum control was the lysate of unstimulated cells measured for total β-hexosaminidase content. Degranulation was calculated as the percentage of β-hexosaminidase released with respect to maximum control (total β-hexosaminidase) after subtraction of negative control (unspecific release) using the formula % degranulation = 100 × (test compound – negative control)/(maximum control – negative control).

Cytotoxicity was determined using a commercially available membrane integrity assay (Promega Cytotox-One).[13] The maximum tolerated concentration (mtc) was defined as the highest concentration tested leading to a mean LDH release of ≤15% of that of the maximum control.

Degranulation hits were determined to be compounds with a degranulation inhibition ≥75%. Subsequently, hits were ranked according to their safety index to select the compounds with the largest margin between desired effect (inhibition of degranulation) and cytotoxicity (compromised membrane integrity). The safety index is the mtc determined in a membrane-integrity assay over the IC_{50} in the degranulation assay (safety index = mtc/IC_{50}).

Endocytosis Assay

HeLa cells were seeded in 384-well plates at ~500 cells/well. After 72 h, compounds were given and incubated for 2 h in the presence of serum. The medium was completely removed and the staining solution was added consisting of DMEM, Penn/Strep, 100 ng mL^{-1} EGF-Alexa 488, and 5 μg mL^{-1} Transferrin-Alexa 647 (Molecular Probes) in serum-free medium for 10 min at 37 °C before fixation with formaldehyde. Nuclei and cytoplasm were stained, respectively, with 0.4 μg mL^{-1} DAPI and 0.2 μM SYTOblue (Molecular Probes).

Triple color images were acquired using an automated spinning disk confocal microscope (OPERA, Evotec Technologies/Perkin-Elmer). Fifteen images were taken per

well. Image analysis and correction were performed using custom-designed image analysis software (see the supplementary information in ref. 6 for more details).

The data were normalized to the median of the negative control wells, DMSO. Significance for each parameter is a z-score of ±2. Strong endocytic regulators shown in bold in **Supplementary Table S3** are those statistically significant in two or more sets of parameters, as described.[6]

Correlation and Enrichment Analysis

Correlation and enrichment analysis was primarily performed similar to the previously published protocol.[14] Briefly, profiles consisting of 32 endocytic parameters for each compound (EGF and Tf parameters 1–15: **Suppl. Table S2**) were correlated to the endocytic profiles of all of the genes present in the genome-wide RNAi data set.[6] Genes with ±0.7 correlation were analyzed for pathway enrichment using WebGestalt.[15,16] The Pathway Commons Pathway was used for the enrichment analysis.

Phosphoprotein Analysis: Meso Scale Discovery Plates

All buffers and solutions used for the phosphoprotein assay were provided by Meso Scale Discovery. Lysis buffer consisted of 150 mM NaCl, 20 mM Tris, pH 7.5, 1 mM EDTA, 1 mM EGTA, and 1% Triton-X-100. Protease, two different phosphatase inhibitor solutions, and PMSF were added freshly each time. The 10X MSD Tris Wash buffer consisted of 500 mM Tris, pH 7.5, 1.5 M NaCl, and 0.2% Tween-20 and was diluted with deionized water to make a 1X solution. MSD Blocker A was made up of bovine serum albumin in Tris wash buffer and was kept at 4 °C for no longer than 1 wk. the 4X MSD Read buffer T was made by diluting in deionized water to make a 1X stock solution.

The analysis of phosphoproteins was performed according to the instructions of each multispot assay by Meso Scale Discovery. Initially, the amount of protein to add per well was determined by testing 5 μg, 10 μg, and 20 μg protein lysate. Reproducibility between experiments and between wells was analyzed to determine one amount of protein to use for each phosphoprotein. We used 5 μg of protein lysate/well for STAT5 and ERK; 10 μg for Akt, p38, and JNK; and 20 μg for GSK3β.

Briefly, MSD plates were first blocked using 25 μL/well with MSD Blocker A. The plates were shaken at 320 rpm for 1 h at room temperature. Lysates were thawed and diluted in complete lysis buffer accordingly.

The plates were washed four times in MSD Tris wash buffer. Twenty-five microliters per well of the lysate was added to the washed plate. The plates were incubated for either 1 h or 3 h at room temperature at 320 rpm according to the manufacturer's recommendations (1 h: Akt, GSK3β,

STAT5; 3 h: ERK, p38, JNK). Afterward, the plates were washed four times with MSD Tris Wash buffer. This was followed by adding 25 μL/well of the respective diluted detection antibody, and plates were incubated for 1 h at room temperature shaken at 320 rpm. Again, plates were washed four times with MSD Tris wash buffer, and 150 μL/well of MSD Read buffer T was added, avoiding introducing any bubbles. The plates were immediately read on a SECTOR Imager 6000 plate reader.

The amount of total protein phosphorylated was expressed as percentage phosphoprotein using the formula % phosphoprotein = 100 × (2× phosphoprotein signal)/(phosphoprotein signal + total protein signal) after subtraction of the background signal. Please note that the numerator is 2× the phosphoprotein signal because the phosphorylated species is captured by both the phosphoprotein-specific and the phosphorylation state-independent (total) antibodies. The 100% control is the sum of phosphoprotein signal plus total protein signal.

Akt1-PH-GFP Localization

RBL-2H3 cells (4×10^4/well) were seeded into a 24-well dish on coverslips. The next day, cells were transiently transfected using a standard protocol with 1 μg Akt1-PH-GFP and 3 μL lipofectamine 2000/well. After 20 h posttransfection, cells were treated with JADO compounds, reference compound, or vehicle (DMSO) for 1 h. Cells were washed quickly once with phosphate-buffered saline (PBS), and 4% paraformaldehyde was added to each well. Cells were fixed for 15 min and washed three times with PBS. Coverslips were stained with DAPI for 30 min for nucleus identification. After another three PBS washes, coverslips were mounted onto glass slides using Mowiol. Coverslips were imaged using the Zeiss Laser Scanning Confocal Duoscan Microscope (63× oil objective, 1.4, 1 Airy unit). For each experiment, at least 15 images were taken per treatment group. Data from three independent experiments were analyzed.

By analyzing the line intensity plot across each cell in individual confocal sections, the relative change in fluorescence intensity at the plasma membrane was determined. The relative fluorescence intensity ratio was calculated using the formula $I_{mb} - I_{cy}/I_{mb} + I_{cy}$, where I_{mb} is the amplitude of the fluorescence intensity signal at the plasma membrane and I_c is the averaged fluorescence intensity of the cytosol.[17] The closer the ratio approaches a value of zero, the less difference there is between the cytosolic and the membrane fluorescence intensity, indicating a decrease in plasma membrane localization of Akt1-PH-GFP.

Statistical analysis was done using KaleidaGraph software. Multiple comparisons were performed against DMSO control using analysis of variance (Holm's method). Statistical significance ($p \leq 0.05$) is indicated in the figures by an asterisk (*).
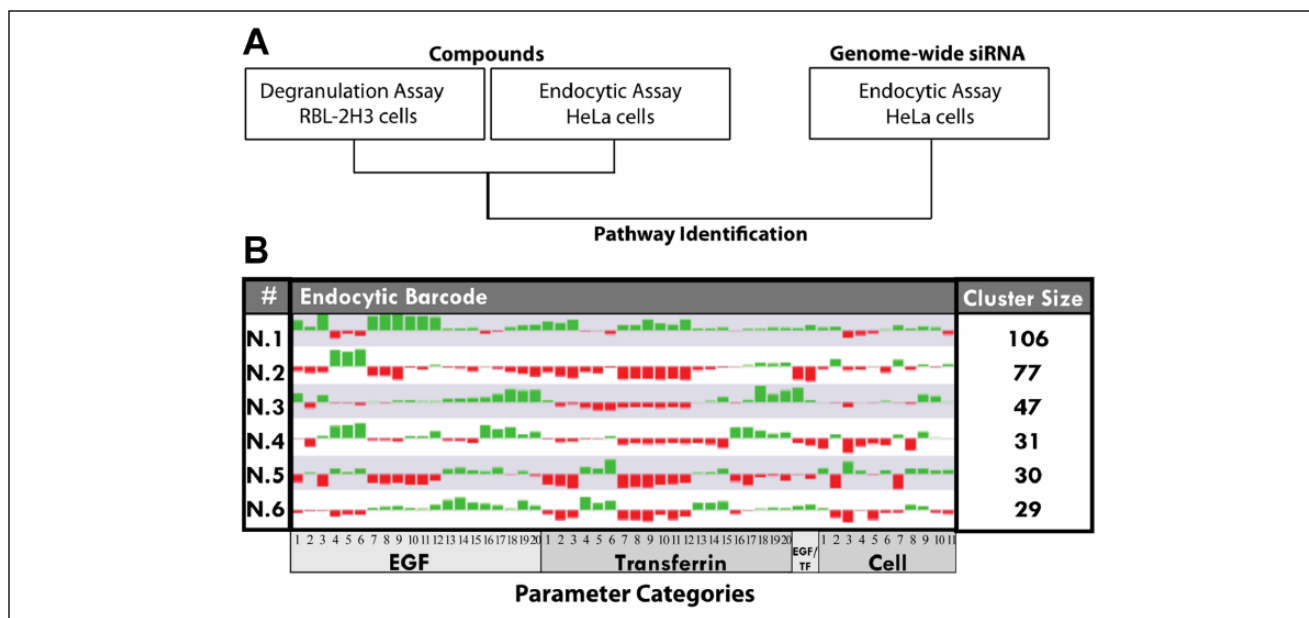
Figure 1. Combinatorial screen analysis to identify hit compounds and pathways. (**A**) Compounds were screened in two different assays: degranulation assay in a mast cell line (RBL-2H3) and in an endocytosis assay for epidermal growth factor (EGF) and transferrin (Tf) uptake in HeLa cells. The endocytic compound profiles were then compared with the previously performed genome-wide siRNA endocytosis screen data set to identify pathways. (**B**) The endocytic profiles of the individual compounds were clustered to group similar profiles with each other. Six clusters (listed under #) were identified, and the endocytic barcode represents the median of each cluster. Each bar corresponds to a specific parameter and is both color and size coded; red indicates a decrease, green an increase, and the size refers to the strength of the difference when compared with the DMSO controls. The number of compounds in each cluster is indicated on the right side of the figure under "cluster size," with the numbers inside the parameter boxes (EGF, Tf, EGF/ Tf, cell) indicating a specific parameter. Legend is located in **Supplementary Table S2**. See **Supplementary Table S4** for a list of compounds in each cluster.

Results

We applied our protocol integrating chemical compounds and computational analysis[7,14] to identify bioactive compounds, predict the biological pathways they modulate, and experimentally validate the predictions. This involved concomitantly screening two assays. One is the query screen for the desired activity (i.e., inhibition of mast cell degranulation), and the second (endocytic assay) is the reference screen, which serves to characterize the compounds with respect to endocytosis, cell health, and pathway identification (overview in **Fig. 1A**).

To identify compounds inhibiting mast cell degranulation, we established a screening library consisting of about 300 compounds. The screening library comprised a representative and chemically diverse subset of a larger compound library containing mainly amphiphilic compounds designed to modulate membrane-associated processes. The compounds were screened in a well-established RBL-2H3 mast cell model for their effect on degranulation. Briefly, RBL-2H3 cells were sensitized overnight with DNP-HSA and, the following day, stimulated with antigen for 15 min. The cells were then lysed, and β-hexosaminidase was measured as a measure of degranulation. Miltefosine has previously been

shown to inhibit mast cell activation in vitro and ex vivo[11,12] and therefore was used throughout this study as our internal reference standard compound. Many compounds were found to inhibit degranulation as effectively or better than the reference compound miltefosine (**Suppl. Table S1**). More than 100 compounds scored as hits, defined as reducing degranulation by $\geq$75%, with miltefosine having 86.8% inhibition. To pragmatically reduce the number to a manageable amount, hits were ranked according to their safety index (**Suppl. Table S1**). We chose the top 60 compounds (defined as the degranulation set), which also preserved sufficient chemical diversity, resulting in a safety index cutoff of 9.2. Miltefosine was indexed at 5.4.

The same library was also screened in the high-content, image-based Tf and EGF endocytosis assay previously applied to a genome-wide RNAi screen[6] to profile the compounds with respect to endocytosis. As in the RNAi screen, quantitative multiparametric image analysis was applied to measure 42 endocytic parameters including the amount of cargo endocytosed, distribution within the endosomal network, and so forth. Moreover, a set of 11 morphological parameters such as cell area, shape, and nuclear size provided information about the general state of the cell and served to exclude compounds with toxic or lethal effects.

Briefly for the endocytosis assay, HeLa cells were plated in 384-well plates and the day after preincubated for 2 h in the presence of the compounds. The controls included DMSO, the EGFR inhibitor (AG1478), and miltefosine. Then, Tf-AF647 (5 μg/mL) and EGF-AF488 (100 ng/mL) were internalized for 10 min, cells were fixed and imaged with an automated spinning disk microscope as described,[6] and the images (15 images per well) were processed. Raw image data can be found in a publicly available database (http://zerial.mpi-cbg.de/page/resources). Initially, multiparametric profiles were generated for each compound and normalized to the median of the DMSO controls. The profiles were visualized as a graph connecting the values of the endocytic parameters classified into four different categories (see **Fig. 1B**; **Suppl. Table S2**; **Suppl. Table S3**). The first two categories comprised cargo parameters (EGF and Tf) such as total amount of cargo (i.e., internalization), the area of vesicles, and the density of cargo per vesicle. The EGF/Tf category comprised the co-localization of the two cargoes whereas the cell parameters included the number of cells, the cell and nuclear sizes, and the shape of the cell. A Venn diagram illustrates the overlap (22 compounds) between strong endocytic regulators (defined as compounds having a statistically significant z-score on two or more parameter sets[6]; **Suppl. Table S3**) and the degranulation set (**Fig. 2A**; **Suppl. Table S1**).

However, the Venn diagram provides only a general comparison of the compounds scoring in the two assays and cannot resolve the effects on specific parameter sets. To classify the compounds on the basis of their activity and specificity in a multiparametric fashion, we grouped the phenotypic profiles of the compounds into classes by performing an unbiased cluster analysis as described previously.[6] Such a clustering method has also been recently used to cluster compounds screened in an image-based assay measuring intracellular killing of *Mycobacterium tuberculosis*.[7] This placed the compounds into six phenotypic clusters (**Fig. 1B**; **Suppl. Table S4**). These clusters represent distinct phenotypes and vary in size between 29 and 106 compounds. Note that clustering was performed on all compounds and not just on hits as in a typical clustering method. This is because we wanted to identify the cluster with a tradeoff between the fewest changes on both the endocytic and cell parameters and the highest activity in degranulation. Because cell toxicity is one of the first aspects monitored in drug discovery, we first focused on the cell parameters. The two clusters with the fewest changes on cell parameters were clusters N.1 and N.3, whereas all other clusters contained strong alterations (**Fig. 1B**; note the size of the bar indicates the strength of the difference). The endocytic parameters of clusters N.1 and 3 were disparate from each other. In cluster N.1, the parameters were consistently altered for both Tf and EGF, suggesting that the compounds have a general effect on the endocytic system. In
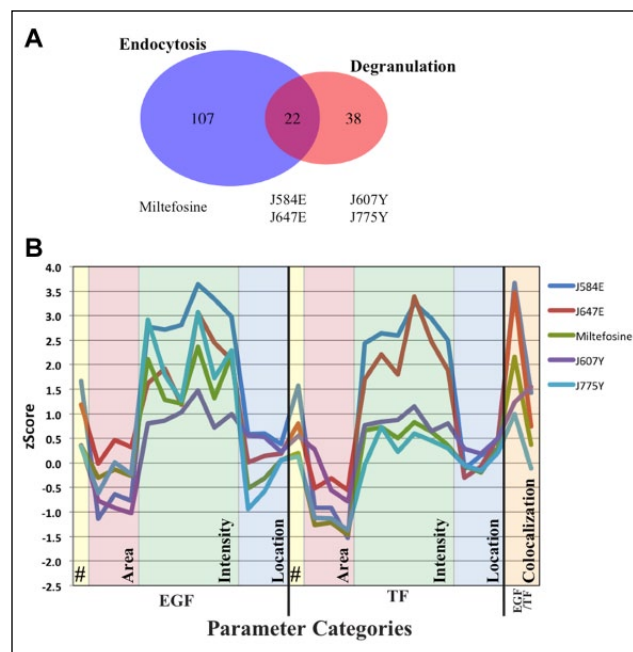
Figure 2. Overview of results and representative endocytic profiles. (**A**) Venn diagram illustrating in blue compounds that scored strongly in the endocytic assay, in orange compounds ranked highly in the degranulation assay, and in red compounds found in both categories. Representatives of each category are listed below the diagram. (**B**) Endocytic profiles of the compounds shown in (**A**) and found in cluster N.1 (J647E, J584E, J775Y, J607Y, and miltefosine). The profiles of J647E and J584E have higher z-scores for more epidermal growth factor and transferrin parameters. Miltefosine also has several parameters with a z-score greater than 2. Statistical significance is a z-score of ±2. Legend is located in **Supplementary Table S2**.

contrast, in cluster N.3, many of the Tf parameters were decreased, suggesting that they affect specifically the early endocytic/recycling pathway. Next, we looked at in which clusters the degranulation set compounds (60 compounds) were found. They were spread among all clusters (**Suppl. Table 4**, underlined and bold compounds), with clusters N.1 and N.3 having the highest number (N.1, 11; N.3, 23). Our reference miltefosine was found in cluster N.1. Representative cluster N.1 compounds from both sets and the overlap in the Venn diagram are highlighted in **Figure 2A**, with their respective endocytic profiles shown in **Figure 2B**. Here, the z-score differences between compounds are visible (compare overlap compounds J584E and J647E to degranulation set compounds J607Y and J775Y). In addition, note the overall similarity between the profiles as they are all found in cluster N.1.

The next step was to predict pathways modulated by these compounds. To this end, we performed a correlation analysis using data from the previous genome-wide RNAi screen (GWS)[6] (data set can be found at http://endosomics.mpi-cbg.de). This is based on the idea that the depletion of
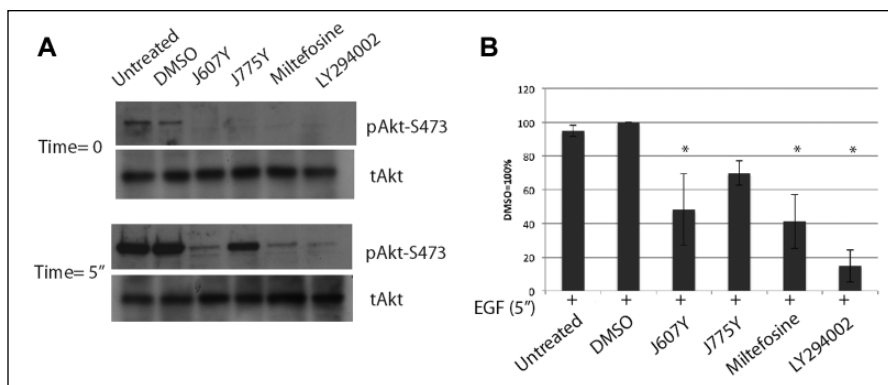
Figure 3. J607Y and J775Y decreased Akt phosphorylation in HeLa cells. HeLa cells were incubated with 25 µM compound for 1 h and stimulated with 100 ng/mL of epidermal growth factor (EGF) for 5 min. Positive control of LY294002 was used at 10 µM. Untreated cells were not stimulated with EGF. (**A**) Representative membranes and (**B**) quantification of membranes. Experiments were repeated three times. Asterisks indicate statistical significance (analysis of variance with Dunnett's post hoc test, $p < 0.05$).

a protein of a particular pathway via RNAi can have a similar profile as a compound inhibiting the same particular protein or pathway. In addition, a negative correlation was also used to identify genes because pathways contain both positive and negative regulators. The endocytic profiles of individual compounds were correlated to the GWS data set using correlation thresholds of ±0.7 (**Suppl. Table S3**). For this analysis, we selected a subset of the compounds containing candidates selected for preclinical development and controls. Again, we took miltefosine as a positive control and as a negative control a compound with no effect on degranulation (J563Y). Several compounds from both clusters N.1 and N.3 that decreased degranulation were analyzed (N1, J607Y, J775Y, J647E; N.3, J656Y and J661Y). J656Y and J661Y were also not strong endocytic regulators (i.e., found only in the degranulation set in the Venn diagram (**Fig. 2A**). A wide range of genes was identified for each compound (**Suppl. Table S5**). To identify pathways targeted by the compound, pathway enrichment from the gene list was performed using the WEB-based Gene SeT AnaLysis (WebGestalt)[15,16] (http://bioinfo.vanderbilt.edu/webgestalt/). Each compound produced a distinct set of significant pathways (**Suppl. Table S6**), with several pathways common between the compounds of cluster N.1, such as "Internalization of ErbB1" and "IL-3 mediated signaling events." Interestingly, the cluster N.1 compounds (miltefosine, J607Y, J647E, and J775Y) all contained several common pathways, whereas the compound with no effect on degranulation (J563Y) and the compounds from cluster N.3 (J656Y and J661Y) produced different enrichment pathway lists (**Suppl. Table S6**). This suggests that the hit compounds from cluster N.1 target similar pathways and that these are distinct from those modulated by compounds from cluster N.3.

The bioinformatics analysis predicted that the compounds affected a set of common pathways. By examining the components of the pathways, Akt was identified most often (**Suppl. Table S6**) and in every analysis of the compounds of cluster N.1, predicting that the Akt pathway and, possibly, its upstream regulators, may be altered. This

prediction is interesting because miltefosine has been shown to affect Akt activity.[18] We tested this prediction by measuring Akt phosphorylation. Because the endocytosis assay was performed in HeLa cells and EGF causes phosphorylation of Akt, we chose to initially examine the levels of Akt phosphorylation in HeLa cells upon stimulation of EGF at various time points in the presence of the representative hit compounds. As predicted, cluster N.1 compound J607Y decreased EGF-stimulated Akt phosphorylation in HeLa cells, whereas J775Y only slightly decreased Akt phosphorylation (**Fig. 3**). The inhibition of Akt phosphorylation with miltefosine is in agreement with an earlier report performed in different cell lines.[18] This suggests that inhibition of degranulation by these compounds leads to suppression of Akt phosphorylation and provides support for our correlation analysis.

The next step was to include additional pathways and compounds to challenge our screening analysis and to perform this in the cell line of original interest, RBL-2H3 cells. To do so, we used a sensitive and robust electrochemiluminescence-based immunological assay (see the Methods and Materials section). This enzyme-linked immunosorbent assay–based assay is set up in 96-well plates and is multiplexed so that the phosphorylated and total protein can be measured simultaneously in the same well (see the Methods and Materials section). In the initial phase, when the experimental conditions were established, the 96-well plates were tested using various amounts of lysate, and the amount of lysate found to provide the most reproducible results was then used for further experiments (for additional information, see the Methods and Materials section). Lysates were prepared from RBL-2H3 that had been sensitized overnight with IgE and then stimulated for 15 min with DNP-HSA, like in the degranulation assay. Syk inhibitor, a known inhibitor of degranulation, was used as positive control.[19] We chose to test both phosphorylated proteins that are known degranulation assay components and of which components of the pathway were found in the pathway analysis (ERK, p38, JNK) and others that were neither identified by the pathway analysis nor established degranulation pathway components (STAT5 and GSK3β). As shown in **Figure 4A and B**, both
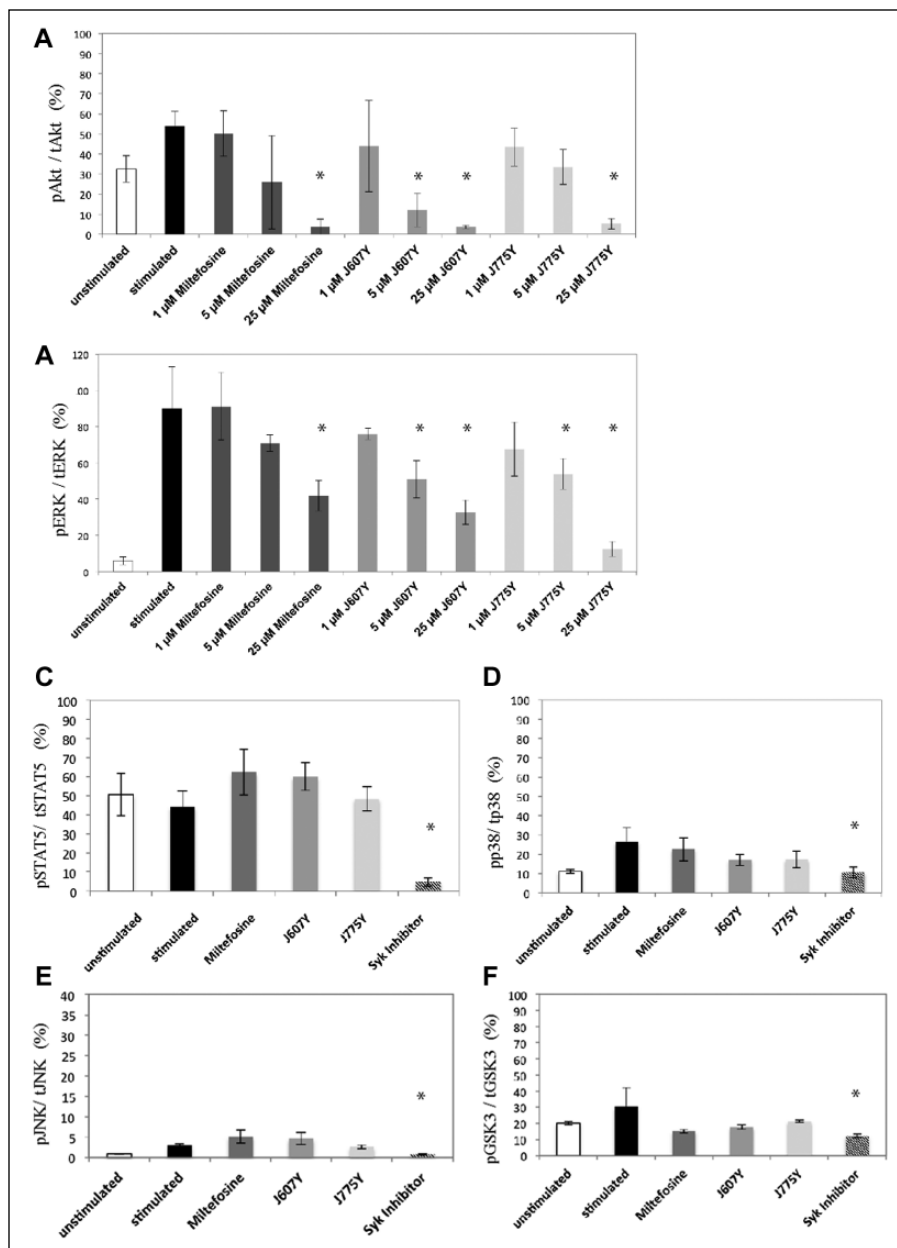
Figure 4. Compounds dose-dependently decreased Akt and ERK phosphorylation in RBL-2H3 cells. RBL-2H3 cells were incubated with 1 µM, 5 µM, or 25 µM compound for 2 h and then stimulated with dinitrophenyl–human serum albumin for 15 min. Cells were lysed, and a specific amount of lysate was tested in the pAkt/tAkt (**A**) and pERK/tERK (**B**) MSD plates. MSD assays were performed using the Syk inhibitor as a positive control. (**C**) pSTAT5/tSTAT5, (**D**) pp38/tp38, (**E**) pJNK/tJNK, and (**F**) pGSK3β/tGSK3β. The amount of total protein phosphorylated was expressed as percentage phosphoprotein as described in the Methods and Materials section. All experiments were performed in triplicate. Asterisks indicate statistical significance (analysis of variance, $p < 0.05$).

J607Y and J775Y inhibited Akt (S473) and ERK phosphorylation in a dose-dependent manner similar to miltefosine. In RBL-2H3 cells, J775Y also had an effect on Akt phosphorylation, which was stronger than in HeLa cells. J607Y also significantly decreased Akt and ERK phosphorylation at 5 µM. Importantly, the phosphorylation of other signaling proteins, STAT5 (**Fig. 4C**), p38 (**Fig. 4D**), JNK (**Fig. 4E**), and GSK3β (**Fig. 4F**) were unaltered. Akt phosphorylation in the presence of the highest concentration of miltefosine, J607Y, or J775Y was reduced to below the unstimulated level. This prompted us to test the compounds in the absence of stimulation. Indeed, under these conditions, the compounds reduced basal Akt phosphorylation (**Supp. Fig. S1A**). Furthermore,

not only was the phosphorylation of S473 of Akt reduced, but the initial phosphorylation site, T308,[20] was also reduced in the presence and absence of stimulation (**Supp. Fig. S1B**). As an additional control, compounds that did not decrease degranulation showed no decrease in Akt phosphorylation (**Supp. Fig. S1C**).

One explanation for the decrease in Akt phosphorylation is the reduced recruitment of Akt to the plasma membrane, the site for activation by PI3K. Akt possesses a pleckstrin homology (PH) domain that specifically binds to phosphatidylinositol (3,4)-bisphosphate (PI(3,4)P$_2$) and phosphatidylinositol (3,4,5)-trisphosphate (PI(3,4,5)P$_3$).[21] Upon receptor activation, PI(4)P and PI(4,5)P2 are converted into
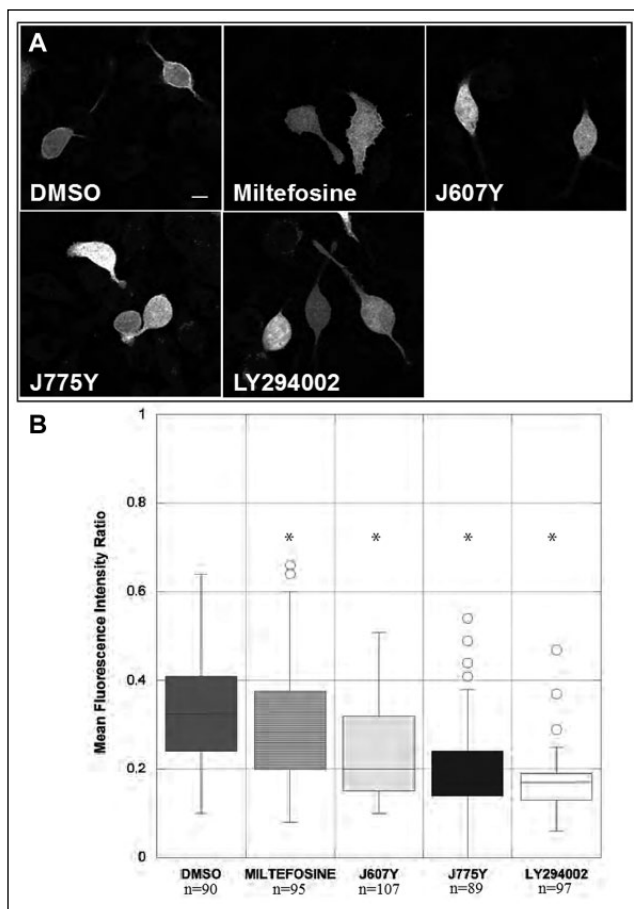
Figure 5. Compounds reduced localization of GFP-Akt1-PH to the membrane in RBL-2H3 cells. RBL-2H3 cells were transiently transfected with GFP-Akt1-PH. Twenty hours after transfection, the cells were treated with 25 μM J607Y, J775Y, or miltefosine and 10 μM LY294002 or DMSO control for 1 h. (**A**) Representative images for each condition are shown. Scale bar is 10 μm. (**B**) The number of cells (*n*) per condition analyzed is indicated below the figure. Asterisks indicate statistical significance (analysis of variance with Dunnett's post hoc test, *p* < 0.05).

PI(3,4)P2 and PI(3,4,5)P3, respectively, by phosphatidylinositol 3-kinase (PI3K), and, via its PH domain, Akt is recruited to the plasma membrane where it becomes phosphorylated by PDK1 at Thr[308] and an additional kinase, either mTORC2[22] or DNA-PK,[23] at Ser[473]. Because of its binding specificity, the PH domain of Akt therefore serves as a useful marker for PI(3,4)P2 and PI(3,4,5)P3.[17] RBL-2H3 cells, transiently expressing the Akt1 PH domain fused to GFP, were used to determine the effect of the hit compounds on plasma membrane localization of the Akt1 PH domain. Miltefosine, J607Y, and J775Y were tested at 25 μM, a concentration shown to effectively inhibit Akt phosphorylation in RBL-2H3 cells. The relative fluorescence ratio was calculated for each fluorescent cell from each confocal image as described in the Methods and Materials section. As expected, the reference compound LY294002, a broad PI3K inhibitor preventing generation of

PI(3,4,5)P$_3$ and PI(3,4)P$_2$ in the plasma membrane, significantly decreased the fluorescence ratio of Akt1-PH-GFP compared with vehicle (DMSO; **Fig. 5A**, representative images, and **Fig. 5B**, quantification). Miltefosine, J607Y, and J775Y significantly decreased the relative fluorescence intensity ratio of Akt1-PH-GFP, with J775Y having the most significant effect. Interestingly, the compounds had a much stronger effect than miltefosine. Overall, this suggests that the level of PI(3,4,5)P$_3$ and PI(3,4)P$_2$ at the plasma membrane is reduced in the presence of the hit compounds, leading to a less efficient recruitment of Akt to the plasma membrane in RBL-2H3 cells.

Discussion

The results shown here highlight the strength and advantages of integrating data from multiple screens and resources. Specifically, the power of this method is the ability to predict pathways modulated by small molecules at an early step during the drug discovery process. The screening library was subjected simultaneously to two assays, one for mast cell degranulation and the other (endocytic assay) as reference for computational analysis. Correlation of the endocytic profiles of the compounds with the corresponding ones of the reference genome-wide RNAi data set predicted pathways that were subsequently validated. The method further corroborates the previous approach[14] using a completely disparate library and biological assay. Overall, we identified two novel compounds that inhibited mast cell degranulation, inhibited Akt phosphorylation, and outperformed our internal reference miltefosine. Importantly, the identification could not have been done with the primary screen alone.

In our study, we focused on the Akt pathway because of the known activation of Akt in mast cell degranulation[24] and Akt regulation via lipid rafts.[25] It is important to note that the compounds J607Y and J775Y exerted an inhibitory effect on the recruitment of Akt-PH to the plasma membrane, arguing that the compounds do not act upon Akt itself but on upstream regulatory components. In addition, we cannot rule out an additional target and/or function of these compounds. Nevertheless, we can rule out major endocytic defects with J607Y and J775Y as shown in the endocytic profiles in **Figure 2** in comparison to J647E and J584E, which significantly altered both EGF and Tf uptake. Interestingly, J607Y and J775Y exerted only modest effects on endocytosis, excluding the possibility that the target(s) of the compounds may be general endocytic regulators.

The main strength of our approach is the use of the genome-wide RNAi data set in the high-content endocytosis assay to select hit compounds and candidate pathways to study further. Our results suggest that the wealth of information from functional genomics screens[26] should be more often used to gain additional insights into the mode of action of small molecules. Although one of the compounds (J607Y) reduced Akt phosphorylation both in HeLa and RBL-2H3 cells, caution should be taken in the interpretation of results when comparing

different cell types and species. Increasing the number of assays, parameters, and cell types will strengthen the resolution and power of the computational approach, providing more accurate predictions and increasing the resolution of the pathway analysis. A second advantage of the image-based cell assays, such as the endocytosis assay, is the ability to assess cell toxicity and morphological changes without the requirement of additional assays. Clearly, the data in vitro alone cannot rule out that there still may be in vivo toxicity.

Overall, our approach highlights the amount of information one can obtain using a multiparametric assay, such as the endocytosis assay, as a reference data set. In the future, by including additional functional genomics screens, the accuracy of the approach can be improved dramatically.

References

1. Arrowsmith, J.; Miller, P. Trial Watch: Phase II and Phase III Attrition Rates 2011-2012. *Nat. Rev. Drug Discov.* **2013**, *12*, 569.
2. Lamb, J.; Crawford, E. D.; Peck, D.; et al. The Connectivity Map: Using Gene-Expression Signatures to Connect Small Molecules, Genes, and Disease. *Science* **2006**, *313*, 1929–1935.
3. Swinney, D. C.; Anthony, J. How Were New Medicines Discovered? *Nat. Rev. Drug Discov.* **2011**, *10*, 507–519.
4. Swinney, D. C. The Contribution of Mechanistic Understanding to Phenotypic Screening for First-in-Class Medicines. *J. Biomol. Screen.* **2013**, *18*, 1186–1192.
5. Singh, S.; Carpenter, A. E.; Genovesio, A. Increasing the Content of High-Content Screening: An Overview. *J. Biomol. Screen.* **2014**, *19*, 640–650.
6. Collinet, C.; Stoter, M.; Bradshaw, C. R.; et al. Systems Survey of Endocytosis by Multiparametric Image Analysis. *Nature* **2010**, *464*, 243–249.
7. Sundaramurthy, V.; Barsacchi, R.; Samusik, N.; et al. Integration of Chemical and RNAi Multiparametric Profiles Identifies Triggers of Intracellular Mycobacterial Killing. *Cell Host Microbe* **2013**, *13*, 129–142.
8. Tsai, M.; Galli, S. J. IgE and Mast Cells in Allergic Disease. *Nat. Med.* **2012**, *18*, 693–704.
9. Rivera, J.; Fierro, N. A.; Olivera, A.; et al. New Insights on Mast Cell Activation via the High Affinity Receptor for IgE. *Adv. Immunol.* **2008**, *98*, 85–120.
10. Molfetta, R.; Gasparrini, F.; Peruzzi, G.; et al. Lipid Raft-Dependent FcepsilonRI Ubiquitination Regulates Receptor Endocytosis through the Action of Ubiquitin Binding Adaptors. *PLoS One* **2009**, *4*, e5604.
11. Weller, K.; Artuc, M.; Jennings, G.; et al. Miltefosine Inhibits Human Mast Cell Activation and Mediator Release Both In Vitro and In Vivo. *J. Invest. Dermatol.*, **2009**, *129*, 496–498.
12. Maurer, M.; Magerl, M.; Metz, M.; et al. Miltefosine: A Novel Treatment Option for Mast Cell-Mediated Diseases. *J. Dermatol. Treat.* **2013**, *24*, 244–249.
13. Batista, J.; Friedrichson, T.; Schlechtingen, G.; et al. Computational Screening for Membrane-Directed Inhibitors of Mast Cell Activation. *Eur. J. Med. Chem.* **2010**, *45*, 2700–2704.
14. Sundaramurthy, V.; Barsacchi, R.; Chernykh, M.; et al. Deducing the Mechanism of Action of Compounds Identified in Phenotypic Screens by Integrating Their Multiparametric Profiles with a Reference Genetic Screen. *Nat. Protoc.* **2014**, *9*, 474–490.
15. Wang, J.; Duncan, D.; Shi, Z.; et al. WEB-Based GEne SeT AnaLysis Toolkit (WebGestalt): Update 2013. *Nucleic Acids Res.* **2013**, *41*(Web Server issue), W77–W83.
16. Zhang, B.; Kirov, S.; Snoddy, J. WebGestalt: An Integrated System for Exploring Gene Sets in Various Biological Contexts. *Nucleic Acids Res.* **2005**, *33*(Web Server issue), W741–W748.
17. Stauffer, T. P.; Ahn, S.; Meyer, T. Receptor-Induced Transient Reduction in Plasma Membrane PtdIns(4,5)P2 Concentration Monitored in Living Cells. *Curr. Biol.* **1998**, *8*, 343–346.
18. Ruiter, G. A.; Zerp, S. F.; Bartelink, H.; et al. Anti-Cancer Alkyl-Lysophospholipids Inhibit the Phosphatidylinositol 3-Kinase-Akt/PKB Survival Pathway. *Anticancer Drugs* **2003**, *14*, 167–173.
19. Lai, J. Y.; Cox, P. J.; Patel, R.; et al. Potent Small Molecule Inhibitors of Spleen Tyrosine Kinase (Syk). *Bioorg. Med. Chem. Lett.* **2003**, *13*, 3111–3114.
20. Alessi, D. R.; Andjelkovic, M.; Caudwell, B.; et al. Mechanism of Activation of Protein Kinase B by Insulin and IGF-1. *Embo. J.* **1996**, *15*, 6541–6551.
21. Watton, S. J.; Downward, J. Akt/PKB Localisation and 3′ Phosphoinositide Generation at Sites of Epithelial Cell-Matrix and Cell-Cell Interaction. *Curr. Biol.* **1999**, *9*, 433–436.
22. Sarbassov, D. D.; Guertin, D. A.; Ali, S. M.; et al. Phosphorylation and Regulation of Akt/PKB by the Rictor-mTOR Complex. *Science* **2005**, *307*, 1098–1101.
23. Feng, J.; Park, J.; Cron, P.; et al. Identification of a PKB/Akt Hydrophobic Motif Ser-473 Kinase as DNA-Dependent Protein Kinase. *J. Biol. Chem.* **2004**, *279*, 41189–41196.
24. Takayama, G.; Ohtani, M.; Minowa, A.; et al. Class I PI3K-Mediated Akt and ERK Signals Play a Critical Role in FcεRI-Induced Degranulation in Mast Cells. *Int. Immunol.* **2012**, 1–6.
25. Lasserre, R.; Guo, X.-J.; Conchonaud, F.; et al. Raft Nanodomains Contribute to Akt/PKB Plasma Membrane Recruitment and Activation. *Nat. Chem. Biol.* **2008**, *4*, 538–547.
26. Schmidt, E. E.; Pelz, O.; Buhlmann, S.; et al. GenomeRNAi: A Database for Cell-Based and In Vivo RNAi Phenotypes, 2013 Update. *Nucleic Acids Res.* **2013**, *41*(Database issue), D1021–D1026.